Biochimica et Biophysica Acta 1847 (2015) 241–247

Contents lists available at ScienceDirect

Biochimica et Biophysica Acta

journal homepage: www.elsevier.com/locate/bbabio

Mapping energy transfer channels in fucoxanthin–chlorophyll protein complex

Andrius Gelzinis [a,b], Vytautas Butkus [a,b], Egidijus Songaila [b], Ramūnas Augulis [b], Andrew Gall [c], Claudia Büchel [d], Bruno Robert [c], Darius Abramavicius [a], Donatas Zigmantas [e], Leonas Valkunas [a,b,*]

[a] Department of Theoretical Physics, Faculty of Physics, Vilnius University, Sauletekio 9-III, 10222 Vilnius, Lithuania
[b] Center for Physical Sciences and Technology, Savanoriu 231, 02300 Vilnius, Lithuania
[c] CEA, Institute of Biology and Technology of Saclay, UMR 8221 CNRS, 91191 Gif-sur-Yvette, France
[d] Institut für Molekulare Biowissenschaften, Universität Frankfurt, Max-von-Laue-Straβe 9, Frankfurt, Germany
[e] Department of Chemical Physics, Lund University, P.O. Box 124, 22100 Lund, Sweden

ARTICLE INFO

Article history:
Received 22 September 2014
Received in revised form 11 November 2014
Accepted 14 November 2014
Available online 20 November 2014

Keywords:
Diatoms
Light-harvesting
Two-dimensional spectroscopy

ABSTRACT

Fucoxanthin–chlorophyll protein (FCP) is the key molecular complex performing the light-harvesting function in diatoms, which, being a major group of algae, are responsible for up to one quarter of the total primary production on Earth. These photosynthetic organisms contain an unusually large amount of the carotenoid fucoxanthin, which absorbs the light in the blue–green spectral region and transfers the captured excitation energy to the FCP-bound chlorophylls. Due to the large number of fucoxanthins, the excitation energy transfer cascades in these complexes are particularly tangled. In this work we present the two-color two-dimensional electronic spectroscopy experiments on FCP. Analysis of the data using the modified decay associated spectra permits a detailed mapping of the excitation frequency dependent energy transfer flow with a femtosecond time resolution.

1. Introduction

During the last two decades, a remarkable progress in ultrafast time-resolved spectroscopy has led to an unprecedented characterization of excitation energy transfer kinetics in a multitude of systems, including the mapping of the very first steps of the photosynthetic process occurring after the capture of a solar photon. Excitation energy cascades have been described for the light-harvesting pigment–protein complexes of photosynthetic bacteria [1–3] and plants [4,5] with femtosecond temporal resolution. On the other hand, excitation energy transfer mechanisms in light-harvesting complexes from diatoms attracted considerably less attention. The evolutionary adaptation to their aquatic (mostly marine) environment has steered these (mostly) unicellular algae to develop a photosynthetic unit with a relatively large absorption cross-section in the blue–green spectral region. On a planetary scale the environmental significance of diatoms should never be overlooked. They are estimated to be responsible for up to a quarter of primary production on Earth [6–8]. Additionally, about 16 gigatons of the organic carbon produced by marine phytoplankton per year is thought to be deposited into the ocean interior, i.e. removed from the atmosphere [6]. This is about one third of total ocean production, whereby diatoms account for 40% of the marine phytoplankton production [8], making them bigger producers than all the rainforests on Earth [7]. So diatoms are not only responsible for a lot of O_2 on this planet, but also for removal of CO_2 from the atmosphere.

In diatoms, the absorption in the blue–green spectral region is usually ensured by the carbonyl-containing carotenoid molecules, such as peridinins or fucoxanthins. The fucoxanthin–chlorophyll protein (FCP) is the main complex responsible for light-harvesting. Characterizing the electronic excitation dynamics in FCP is a particularly challenging task because of a large number of molecules and electronic levels involved. As fucoxanthin (Fx) is a carbonyl-containing carotenoid, an intramolecular charge transfer (ICT) state is present in the vicinity of the Fx S_1 state which strongly influences the excited state dynamics [9]. FCP shares structural and sequence homology with the LHCII complex from higher plants [10] and this has led to several models of pigment organization in FCP [11–13]. However, the pigment composition and function in LHCII and FCP are markedly different, as the latter contains nearly as many fucoxanthin molecules as chlorophylls *a* and *c* [11,14,12]. The best characterized fraction of FCP complexes contains no less than 8 molecules of Fx. Together with two protein-bound chlorophyll *c* (Chl *c*) molecules, they confer to the FCP its efficient absorption in the blue–green spectral region (Fig. 1).

In most pump–probe studies of dynamical processes in FCP [11,13,15,16] the 18,000–21,000 cm^{-1} region was excited to populate selectively the Fx S_2 state avoiding the Soret band of the chlorophylls

* Corresponding author at: Center for Physical Sciences and Technology, Savanoriu Avenue 231, LT-02300 Vilnius, Lithuania. Tel.: +370 5 231 3769.
E-mail address: leonas.valkunas@ff.vu.lt (L. Valkunas).

http://dx.doi.org/10.1016/j.bbabio.2014.11.004
0005-2728/

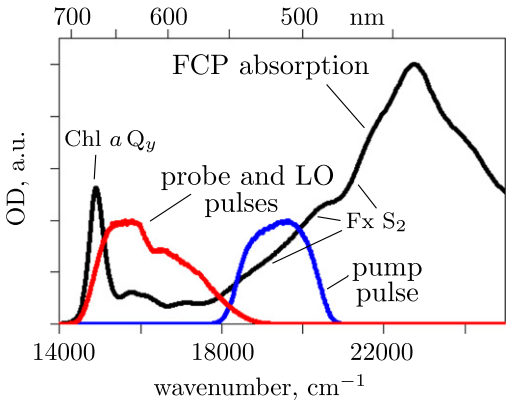

Fig. 1. FCP absorption spectrum (black line) and laser pump, probe and LO spectra used in the two-color 2D experiments (blue and red lines, respectively).

(Fig. 1). Probing at low energies allows one to follow the excitation delivery to the Q_y state of Chl *a*; while most of the excitation of the Fx S_2 state relaxes to the S_1/ICT state in less than 100 fs, a part of the S_2 population is immediately transferred to Chl *a* (within 100–200 fs). The S_1/ICT state undergoes vibrational relaxation on the timescale between 0.5 and 1 ps at the same time transferring energy to Chl *a*. The remaining excitation of the S_1/ICT state then decays to the ground state with a longer timescale (15 to 35 ps). Some spectroscopic measurements suggested the existence of multiple species of Fx, yet their distinct roles have not been explored in detail, partly due to the dependence of frequency and time resolutions in the pump–probe technique. Therefore, a comprehensive scheme of excitation energy transfer cascade remains unavailable.

Coherent two-dimensional (2D) electronic spectroscopy (ES) provides a wealth of information about the energy and charge transfer dynamics, exciton diffusion and relaxation in molecular systems [1,2,4,5,17–20,3,21,22]. In the 2D ES the temporal and spectral resolutions are not related [23], providing a huge advantage over the pump–probe techniques. Usually in the 2D ES, all the excitation pulses are of the same wavelength, or color. However, it may be hugely advantageous to tune them to different wavelengths, thus providing a way to monitor energy transfer between energetically remote excited states [24,25]. This is why in this study we employed the two-color 2D ES to disentangle the complex energy transfer cascades in FCP following the excitation of the Fx S_2 state. Application of the two-color 2D ES is very rare due to its extreme experimental difficulty [24,26–29]. This work is the first application of the two-color 2D ES to a complicated light-harvesting complex. As a result, a comprehensive scheme of energy transfer cascade in FCP following the Fx S_2 state excitation was constructed. It turns out that, although fucoxanthin absorption is stretched over a very large range of energy in these complexes, their spatial organization results in an ultrafast and efficient excitation transfer funnel from any of these molecules to the chlorophylls.

2. Materials and methods

2.1. Sample preparation

Sample preparation is described in detail elsewhere [30]. In short, cultures of the diatom *Cyclotella meneghiniana* were grown under cycles of 16 h light and 8 h dark conditions. FCP complexes were purified by sucrose density centrifugation after solubilization of the thylakoid membranes in the presence of 20 mM dodecylmaltoside. The FCP fractions corresponding to FCPa were harvested and pooled and stored until required.

2.2. 2D ES and pump–probe experiment

For the two-color 2D ES experiment, a diffractive-optics-based non-collinear four-wave mixing setup with phase-matched box geometry, heterodyne detection, and inherent phase-stabilization was used [31,32]. The light source consisted of two non-collinear optical parametric amplifiers, one home-built and one Orpheus (Light Conversion), pumped by an Yb:KGW laser (Pharos, Light Conversion). The pulse repetition rate used in the experiments was 50 kHz. The setup provided 625 nm (100 nm FWHM) 15 fs light pulses and 517 nm 22 fs light pulses (51 nm FWHM, see Fig. 1). Additional sensitivity and noise reduction was achieved by means of a double modulation lock-in detection [32]. The coherence time delay (t_1) was scanned within the −105–132 fs interval with a 1.5 fs time step by deploying movable fused-silica wedges. The population time delay t_2 was scanned using a mechanical delay stage. Measured data sets contained 40 spectra from 0 fs to 500 ps. Modified decay associated spectra fits were performed using 32 spectra up to 100 ps. Spectrometer and dispersive delay line calibration were performed using procedures described in Ref. [33]. The total energy of the sample irradiation was 1 nJ/pulse, the diameter of the focused beam at the sample was ~100 μm. To avoid local degradation of the sample at room temperature, a low volume fused silica flow cell with 0.2 mm thick windows and 0.2 mm sample chamber was used. The optical density of the sample at 680 nm was about 0.3. The frequency resolution was ~200 cm^{-1} in ω_1 and ~50 cm^{-1} in ω_3. A window function could be applied to remove the wiggles in the 2D spectra, but at a cost of ω_3 range. Thus, we chose not to use it. Pump–probe experiments were performed using essentially the same setup, just blocking two out of four laser pulses (pulses 2 and 3) and using the remaining ones as the pump (pulse 1) and probe (local oscillator) pulses.

3. Principles of two-color 2D ES

In the two-color 2D ES, the wavelengths (colors) of each laser pulse are tuned. Since the narrow-bandwidth laser pulse can trigger the resonant transitions between the electronic states, one can deduce that a wisely chosen sequence of pulse colors in the 2D ES can induce one or more specific excitation evolution pathways. This would allow extracting a specific spectral feature in 2D electronic spectrum (diagonal peak or a cross-peak) determined purely by the pulse energies and spectral bandwidths [25,34]. Here we consider the "populations-specific" two-color 2D ES experiment where the first two excitation, or pump, pulses are resonant with transitions to the high-energy state of an arbitrary system, and the frequency of the third excitation, or probe, pulse and the local oscillator (LO) pulse (which is used in the heterodyne detection [34,35,31,32]) are resonant with the transitions to the lower-energy state. A basic scheme of the experimental setup is presented in Fig. 2a; the delay between the first two pulses is denoted as t_1 (coherence time), between the second and the third as t_2 (population time), and between the third and the signal as t_3 (detection time). A 2D spectrum is obtained by performing the two-dimensional Fourier transform of the signal over delays t_1 and t_3. The Fourier frequencies ω_1 and ω_3 are denoted as the excitation and emission frequencies, respectively. The 2D spectra are then plotted against the excitation (horizontal) and the emission (vertical) axes at fixed values of the population time t_2.

In order to discuss the typical outcomes of the two-color 2D ES experiment, a simple model system of four bands of states can be considered, with an electronic ground state $|g\rangle$, a band of high-energy "blue" states $|B\rangle$, a band of low-energy "red" states $|R\rangle$ and a band of doubly-excited states $|f\rangle$. The schematic energy level diagram and absorption spectrum of this system are presented Fig. 2b along with the spectra of "blue" pump, "red" probe, and LO laser pulses. The system can be optically excited from its ground state $|g\rangle$ to states in either band $|B\rangle$ or band $|R\rangle$. The $g \leftrightarrow B$ transitions are resonant with the pump pulses, while the $g \leftrightarrow R$ and $R \leftrightarrow f$ transitions are resonant with the probe pulse. We assume that the population of the $|B\rangle$ state ($|B\rangle\langle B|$)

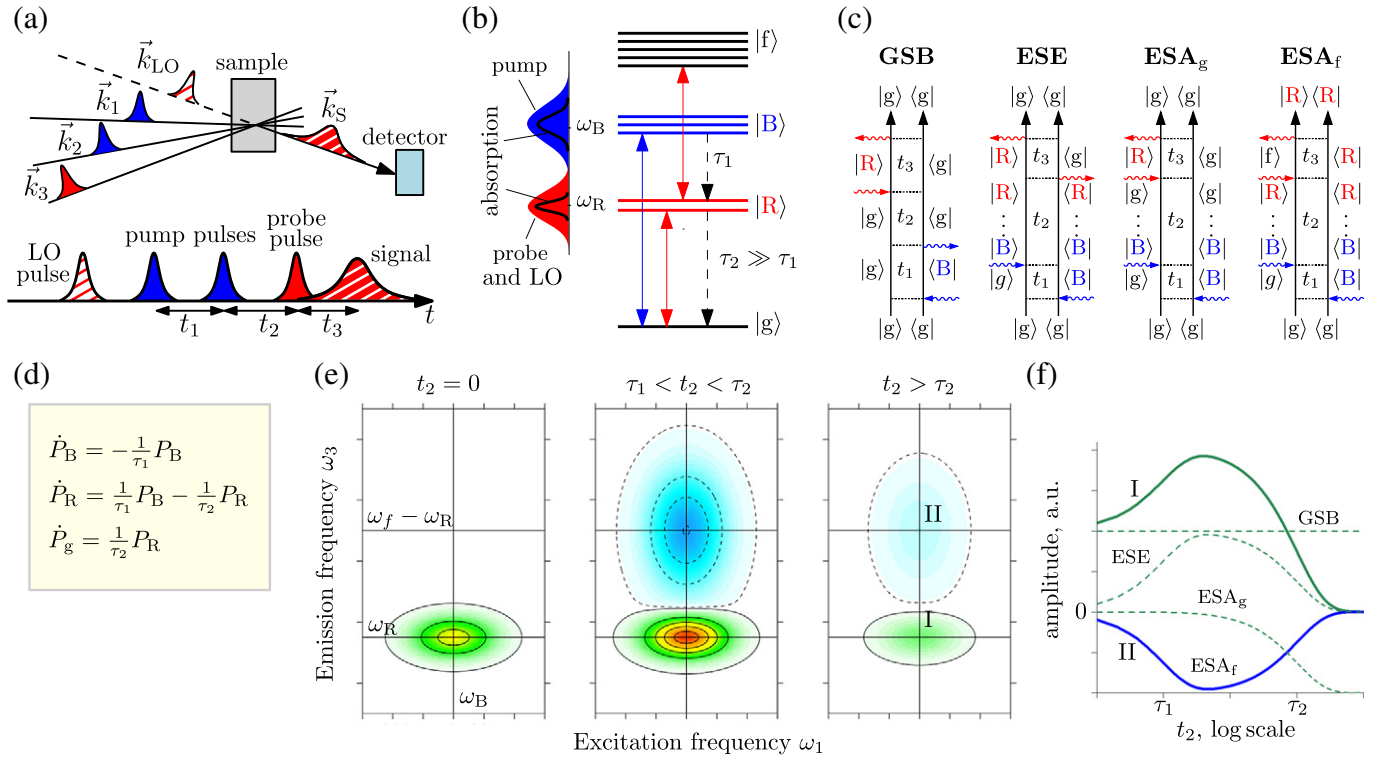

Fig. 2. Overview of the two-color 2D ES technique. (a) Simplified experimental scheme. (b) Energy level scheme of a simple model system with its absorption spectrum and spectra of laser pulses. (c) Double-sided Feynman diagrams contributing to the rephasing two-color 2D spectra. (d) Kinetic equations for populations of the states. Here P_R, P_B, and P_g correspond to populations of the |R⟩, |B⟩, and |g⟩ bands respectively. (e) Two-color 2D ES spectra at different population times t_2. (f) Time evolution of positive (I) and negative (II) peaks (solid lines) and contributions to the former from the distinct Feynman diagrams (dashed lines).

decays to the |R⟩⟨R| state with the rate τ_1^{-1} and that the population |R⟩⟨R| decays to the ground state with rate $\tau_2^{-1} \ll \tau_1^{-1}$.

The processes contributing to the evolution of the peaks in the 2D spectrum can be conveniently assigned to specific double-sided Feynman diagrams, which schematically show the dynamics of the system density matrix [35,34]. They are classified as the ground state bleaching (GSB), excited state emission (ESE) and excited state absorption (ESA) contributions. Since the population of the |B⟩ state decays both to the |R⟩ state (directly) and to the ground state (indirectly), two distinct ESA diagrams (denoted as ESA$_f$ and ESA$_g$, respectively) have to be considered, involving both population relaxation pathways. Therefore, four Feynman diagrams, shown in Fig. 2c, describe the two-color spectrum of our simple model system. Note that these are the so-called "rephasing" diagrams; the "non-rephasing" [23,25,34] diagrams differ only in the order of the first two pulses and do not reflect any new physics in the case considered here. These diagrams depend on population time t_2, representing the evolutions of the populations of the corresponding states; ESA$_g$ contribution depends on the population of the ground state $P_g(t_2)$, while ESE and ESA$_f$ contributions are proportional to the population of the |R⟩ state $P_R(t_2)$. GSB diagram remains constant throughout the entire evolution. The kinetic equations for the populations can be easily formulated and are given in Fig. 2d.

The two-color 2D spectra of our four-band model system are shown in Fig. 2e at three different population times. They contain two distinct features: a positive peak at excitation frequency $\omega_1 = \omega_B$ and emission frequency $\omega_3 = \omega_R$, and a negative peak at $\omega_1 = \omega_B$, $\omega_3 = \omega_f - \omega_R$. Peak widths are influenced by the different number of states in bands |B⟩, |R⟩ and |f⟩.

The time-dependent traces of the maxima of the positive and negative peaks are shown in Fig. 2f by the solid lines; contributions from the distinct Feynman diagrams are shown by the dashed lines. The rise of the negative peak is determined solely by the excited state absorption (ESA$_f$) contribution, when the first two pulses create a |B⟩⟨B| band population, which relaxes to |R⟩⟨R| in time t_2. The positive feature has more contributions: GSB, ESE and ESA$_g$. GSB is responsible for the presence of this peak at the initial population time and ESE causes an increase of the amplitude of this peak at times $\tau_1 < t_2 < \tau_2$. This diagram decays due to the relaxation of the |R⟩⟨R| population to the ground state. An overall peak decay to zero is caused by the cancellation of the constant GSB contribution with the ESA$_g$ diagram.

The analogy between the model system considered here and FCP can be easily drawn in a following way. The Fx S_2 state would correspond to the |B⟩ band, and both Fx S_1/ICT and Chl *a* Q_y states would correspond to the |R⟩ band. The time dependencies of peak intensities will provide direct information about the excitation relaxation pathways and rates in the FCP in a very similar way as in the simple four-band model system.

4. Results

A selection of the two-color 2D spectra of the FCP at different population times is presented in Fig. 3a and two cross-sections of the $t_2 = 3$ ps spectrum at excitation frequencies $\omega_1 = 19{,}000$ cm^{-1} and 20,000 cm^{-1} are shown in Fig. 3b. The negative features at ω_3 from 15,100 to 17,400 cm^{-1} can be assigned to the ESA of the Fx S_1/ICT state with some contributions from the ESA of Chl *a* Q_y at $\approx 15{,}100$ cm^{-1} while the positive band at $\omega_3 \approx 14{,}900$ cm^{-1} corresponds to the ESE from the Chl *a* Q_y band [11,15,16].

A very strong positive peak is visible at the excitation frequency $\omega_1 \approx 19{,}000$ cm^{-1} and emission frequency $\omega_3 \approx 16{,}400$ cm^{-1} at zero population time. This feature disappears at population time $t_2 =$ 50 fs and should be related to the fifth-order response, non-resonant and/or the pulse overlap effects, as it is not observed in the 0 fs two-color pump–probe spectrum, see green line in Fig. 3b (the broad-band pump–probe corresponds to the integral of the 2DES spectrum along ω_1 [23]). Therefore, we do not consider this peak in our analysis. In

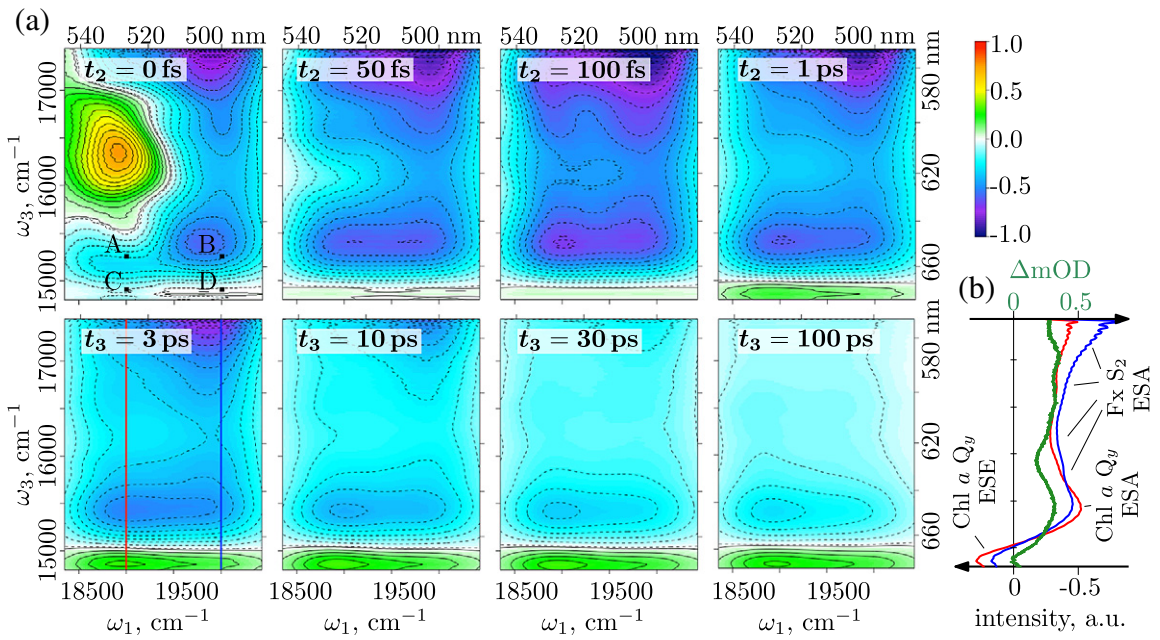

Fig. 3. Two-color 2D spectra of FCP complex at 293 K and their vertical cross-sections. (a) 2D spectra at several population times. The spectra are scaled to the maximum value of the spectrum at $t_2 = 50$ fs. Real (absorptive) part of the total (rephasing + non rephasing) spectra is shown. (b) Cuts of the $t_2 = 3$ ps spectrum along the emission ω_3 axis corresponding to excitation frequency of 19,000 cm^{-1} (red line) and 20,000 cm^{-1} (blue line), and pump–probe spectrum at 0 fs (green line). Note that strong positive feature in $t_2 = 0$ fs 2D spectrum is not observed in the pump–probe data. The wiggles in the 2D spectra arise due to the fact that probe pulse spectrum is broader than the spectrometer spectral range.

addition, we only present those parts of the spectra which are covered by at least 1/e of the maximum of the laser pulse intensity. This secures us from over-analyzing weak features in the spectra, usually leading to misinterpretations.

Time-dependent traces of a few selected peaks (indicated as A, B, C, and D in Fig. 3a) are presented in Fig. 4. The A and B peaks correspond to the ESA of Fx S_1/ICT and Chl *a* Q_y, while peaks C and D correspond to Chl *a* Q_y ESE. The negative ESA features show an initial fast rise and subsequent decay whereas the positive peak of the Chl *a* Q_y shows multiple growth timescales and a very slow decay. Since at $t_2 = 100$ ps the population of the Fx S_1/ICT state is fully relaxed to the ground state in solution [9], the remaining negative features are solely due to the ESA of the Chl *a* Q_y, the lifetime of which is known to be on the order of nanoseconds in FCP [11,16]. No contribution from Chl *c* Q_y and Q_x or from Chl *a* Q_x is observed in our data.

Comparison of time dependencies of A with B, and C with D, reveals that the spectral evolution is dependent on the excitation energy (ω_1), implying the existence of at least two functional fucoxanthin species in the FCP. In order to simplify the discussion, we denote the $\omega_1 < 19{,}500$ cm^{-1} and $\omega_1 > 19{,}500$ cm^{-1} as the excitation regions of Fx_{red} and Fx_{blue} species, respectively.

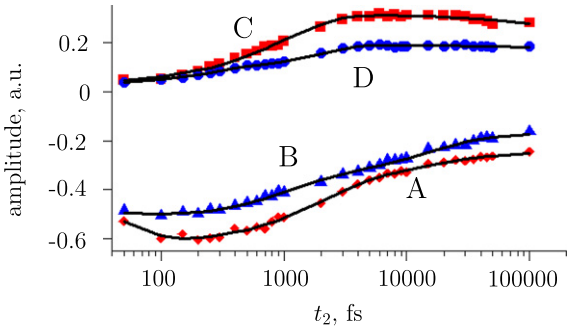

Fig. 4. Time-dependent traces of the selected peaks of the 2D spectra (see Fig. 3a) and their fits obtained from the construction of the modified decay associated spectra (black lines).

Temporal evolution of the spectrum can conveniently be represented by different sorts of decay associated spectra (DAS). Standard DAS analysis of the 2D spectra [36–38], which is similar to the global analysis of the pump–probe spectra [39], is a powerful tool to find out the timescales of the dominant processes in the system. However, it assumes the same decay constants for all data points in spectrum and, thus, it is not suitable for resolving the differences in dynamics upon excitation of Fx_{red} or Fx_{blue} in the 2D spectra of FCP. Instead, we consider the modified decay associated spectra (MDAS) [5], which is constructed by fitting the time evolution of each point in the 2D spectrum by a sum of four decaying exponentials, and allowing the variation of all free parameters of the fit to be independent for each data point. This approach allows us to derive a whole spectral distribution of the decay constants. A four-exponential fit was chosen because attempts to fit the spectra with smaller number of exponentials proved to be unsatisfactory. The fitting was done using the nonlinear optimization algorithm based on the gradient projection method [40], as implemented in the R software [41]. To ensure that the global minimum was reached, the fits were repeated 15 times with different initial conditions. Since the 2D spectra at long times (> 100 ps) show only slow decay on the order of nanoseconds, we used only times up to 100 ps for the fit and set the timescale of the last exponential to 2 ns, as in Ref. [5]. All other timescales and all the amplitudes were not constrained in the fit.

Apart from the nanosecond evolution of the spectrum, we discerned three clusters of shorter timescales. They are represented in MDAS-1 through MDAS-3 and their histograms are shown in the first row of Fig. 5. The maps that correspond to their timescales and amplitudes are presented in the second and third rows, respectively. The fourth decay constant was the same for all points (2 ns), therefore we show only the amplitude map for MDAS-4. Since the sign of the amplitude might be misleading as, e.g. positive amplitude would mean increase of negative signal but decrease of positive signal, we show only the absolute values of the amplitudes. To show the quality of the fit in Fig. 5 we plot the coefficient of variation of the root mean square deviation (RMSD), which is RMSD divided by the mean of observed values. It can be seen that it is smaller than 0.1 at most of the points of the spectrum — points where this value is higher were excluded from further

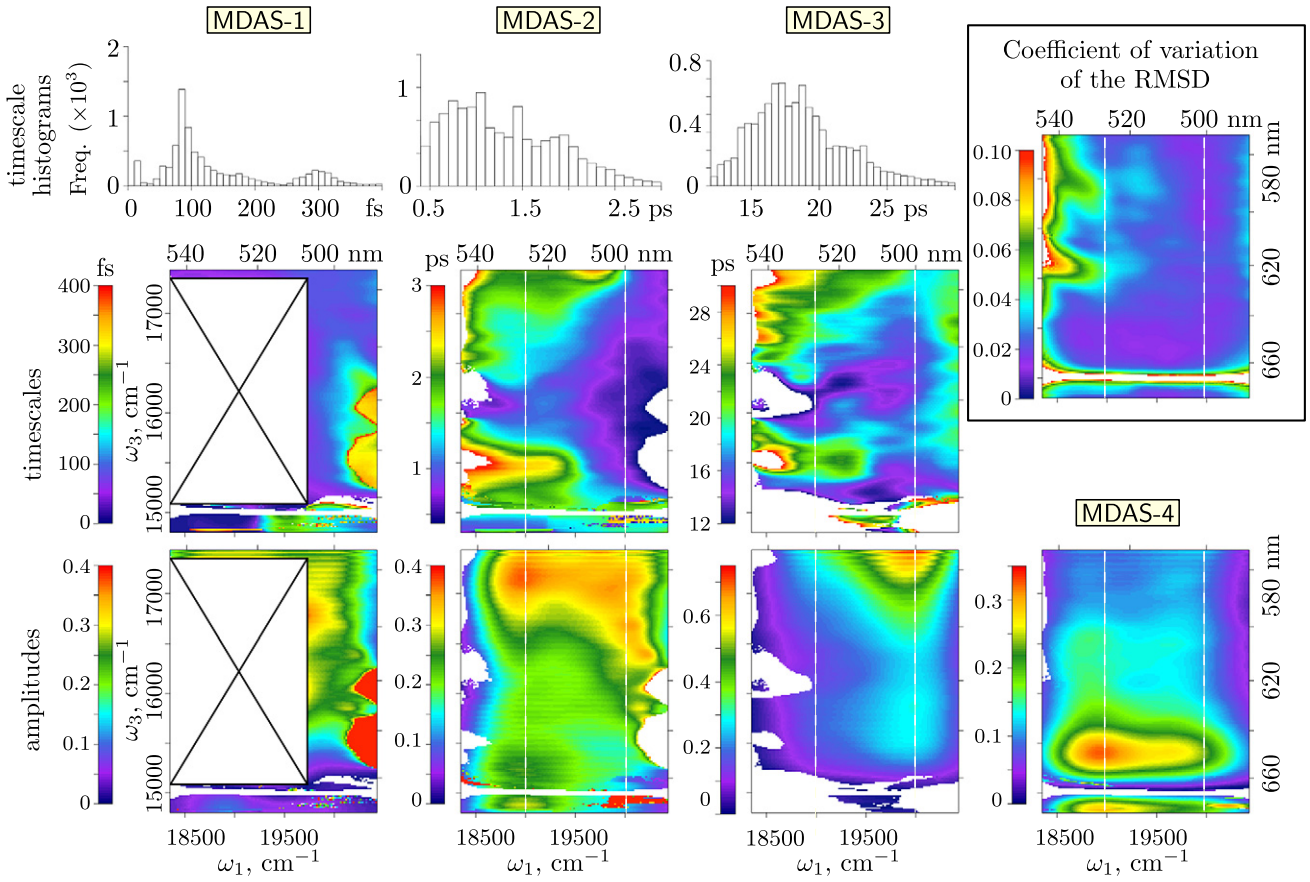

Fig. 5. Modified 2D decay associated spectra of the FCP complex. The first row shows timescale distribution histograms. The second and third rows show timescale and amplitude maps for separate time constant clusters, respectively. Absolute values of the amplitudes are depicted. Amplitudes exceeding the maximum value of the color bar are depicted with the color of maximum allowed value (red). Since the 2D spectrum at $t_2 = 0$ fs is contaminated by the presence of the strong positive peak, it affects the short time dynamics, thus we did not analyze the areas marked by white rectangles in the MDAS-1 plots. The inset shows the coefficient of variation of the root mean square deviation (RMSD) of the fit — points in the spectra where this error exceeded 0.1 were removed from MDAS plots.

analysis. Additionally, the quality of the fit is demonstrated for selected points in Fig. 4.

MDAS-1 (first column in Fig. 5) illustrates the ultrafast processes on timescales shorter than 400 fs. After excitation of the Fx_{red} species ($\omega_1 <$ 19,500 cm^{-1}) we observed < 50 fs processes (we cannot resolve the exact timescale of these processes with certainty) in the Chl *a* Q_y ESE ($\omega_3 \approx$ 14,900 cm^{-1}) and S_1/ICT ESA regions ($\omega_3 \approx$ 17,400 cm^{-1}). The rates of S_2 to S_1/ICT internal conversion and energy transfer from S_2 to Chl *a* must, therefore, be similar. Note that in this MDAS we excluded the region affected by the decay of the positive feature at zero population time (Fig. 3a). Excitation of Fx_{blue} ($\omega_1 >$ 19,500 cm^{-1}) leads to slower evolution in the Chl *a* Q_y ESE region as the signal there grows with a timescale between 100 and 200 fs. The S_1/ICT ESA region ($\omega_3 \gtrsim$ 15,100 cm^{-1}) evolves with times < 100 fs, again indicating efficient internal conversion.

Processes with timescales between 0.4 ps and 3 ps are represented by MDAS-2 (second column in Fig. 5). Again, Fx_{red} and Fx_{blue} spectral regions show different timescale values. After excitation of the Fx_{red} a 0.9–1.2 ps growth component was observed in the Chl *a* Q_y region ($\omega_3 \approx$ 14,900 cm^{-1}), while the decay constants of the S_1/ICT ESA region ($\omega_3 \gtrsim$ 15,100 cm^{-1}) are 1–3 ps. The S_1/ICT ESA showed faster 0.5–2 ps evolution when the Fx_{blue} is excited, and the evolution of Chl *a* Q_y region was slower (1.2–1.6 ps). The amplitude map of MDAS-2 revealed that changes in the Chl *a* Q_y region are more significant when Fx_{red} is excited. Note that two processes contribute to the S_1/ICT dynamics in this timescale window, namely vibrational cooling of the hot Fx S_1/ICT state and energy transfer to chlorophylls. Our analysis did not allow us to distinguish between these processes, thus, we could not estimate the vibrational cooling rate nor determine whether excitation transfer to Chl *a* occurs via hot or relaxed S_1/ICT states.

Processes with timescales between 12 ps and 40 ps are given by MDAS-3 (third column in Fig. 5). The decay timescales of 15-20 ps are slightly faster when the Fx_{blue} is excited, compared to the 15–28 ps timescales obtained upon the Fx_{red} excitation. The amplitude map shows that this decay is much stronger upon Fx_{blue} excitation, implying that overall transfer efficiency to Chl *a* is lower for Fx_{blue}.

The slowest processes are illustrated by MDAS-4 with a fixed timescale of 2 ns (see above). The amplitude map shows long time decay of the Chl *a* Q_y ESE and ESA bands.

5. Discussion

Two-color two-dimensional electronic spectroscopy performed on a photosynthetic protein from diatoms clearly distinguishes “red” and “blue” functional species of fucoxanthin and reveals that their excitation results in qualitatively distinct spectral evolutions. From the 2D spectra and subsequent MDAS analysis we can conclude that their S_2 energies correspond to transitions at approximately 19,000 cm^{-1} and 20,000 cm^{-1}, respectively. It was recently shown that three Fx species could be distinguished in FCP [14], based on their resonant Raman properties. Our results indicate that two of these species are preferably excited at 19,000 and 20,000 cm^{-1}, without much excitation of the other species. The existence of a third Fx species would be consistent with our data if its excitation energy was > 20,500 cm^{-1}, that is not covered with our pulses.

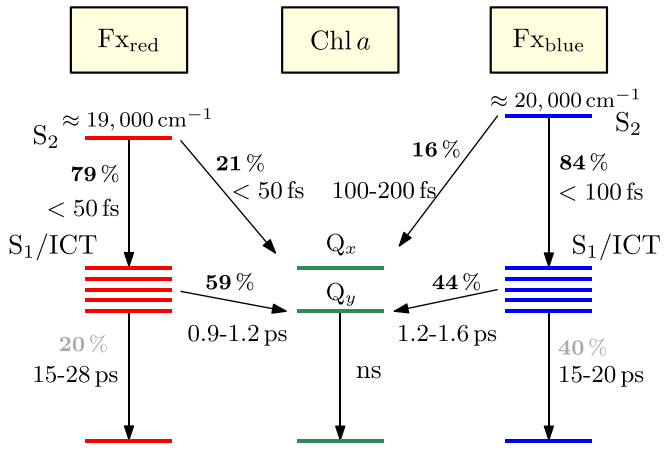

Fig. 6. Scheme of the energy transfer pathways in the FCP complex obtained from the two-color 2D spectra and modified decay associated spectra.

With all this in mind, we construct a comprehensive energy transfer cascade scheme for the FCP that includes both Fx species (Fig. 6). While the timescales were obtained from the MDAS analysis, the relative amplitudes were obtained as follows. From the FCP fluorescence excitation spectrum given in Ref. [11] the overall transfer yield after Fx$_{red}$ and Fx$_{blue}$ excitation was estimated to be 80% and 60%, respectively. The ratios of the S_2 to Chl *a* and S_1/ICT to Chl *a* transfer were obtained from MDAS-1 and MDAS-2 (Fig. 5) and the remaining amplitudes were derived from the compartmental model as $A_{S_1/ICT \leftarrow S_2} + A_{Chl\ a \leftarrow S_2} = 1$ and $A_{Chl\ a \leftarrow S_1/ICT} + A_{S_0 \leftarrow S_1/ICT} = A_{S_1/ICT \leftarrow S_2}$.

Our energy transfer scheme in Fig. 6 shows the major excitation relaxation pathways. Some excitation energy is transferred from both Fx$_{blue}$ S_2 and Fx$_{red}$ S_2 to Chl *a*. This transfer is slower for Fx$_{blue}$. Nonetheless, most of the excitation from the Fx$_{blue}$ S_2 and Fx$_{red}$ S_2 states relaxes to their respective S_1/ICT states within 100 femtoseconds. From there, Fx$_{red}$ transfers most of its excitation (59%) to Chl *a*, while this transfer is slightly less efficient from Fx$_{blue}$ (44%). This transfer step is again slower for Fx$_{blue}$. Hence, the Fx$_{red}$ pigments should either be more strongly coupled to the Chl *a* pigments (being closer or having a more favorable orientation) or their electronic states must be closer in energy to the Chl *a* states, since, as reported earlier [13], the excitation transfer is faster from those pigments both from S_2 and S_1/ICT states. However, 20% (Fx$_{red}$) or even 40% (Fx$_{blue}$) of excitation is not transferred to chlorophylls, but relaxes to the ground state. This might be surprising, since the transfer rates from S_1/ICT to Chl *a* Q_y are much faster than decay to the ground state, and only a small fraction of excitation population should be lost as a result of the latter process. However, transfer rates and amplitudes in our scheme represent averaged values, which are greatly affected if the Fx molecules in the whole complex are scattered around the complex. The existence of at least one poorly transferring Fx$_{blue}$ is consistent with previous suggestions [11,13] and with the amplitude map of MDAS-3 in Fig. 5. Also, we note that the direct interaction between the S_1/ICT states of Fx$_{red}$ and Fx$_{blue}$ must be weak, because they decay to the ground state with distinct lifetimes whereas strong interaction would lead to decay with the same rate [42,43].

Photosynthetic pigment–protein complexes of diatoms and other underwater organisms are adapted to significantly different light conditions if compared with plants [44]. This can be seen by comparing the absorption spectra of the corresponding complexes: while the strong Chl *a* Q_y absorption band in the LHCII can provide a large portion of photons for the plants, its importance quickly diminishes in underwater conditions due to the different solar spectra. Indeed, fucoxanthins in FCP absorb more efficiently in the "green gap" where chlorophylls absorb poorly, yet there are relatively more green photons in underwater. The pigment organization in FCP then results in fast overall energy transfer from fucoxanthins to chlorophylls using pathways from both S_2 and S_1/ICT states. The energy transfer efficiency of 80% from red fucoxanthins is similar to transfer efficiency from carotenoids in LHCII [45,46], while it is somewhat less efficient from blue fucoxanthins (60%). Note that in the present work we considered isolated FCP complexes. However, experiments done on the whole cells of diatoms indicate that different Fx species might have different responsibilities in the overall energy transfer network, as Fx$_{red}$ was suggested to transfer more to PSII and Fx$_{blue}$ to PSI [47,48].

Although we have recently demonstrated an ultrafast (~ 60 fs) energy transfer from Chl *c* to Chl *a* in the FCP [49], we could not extract any spectral features involving the Chl *c* from this set of measurements. Nonetheless, if the excitation is transferred from Fx to Chl *c*, it would be further transferred to Chl *a* very rapidly. In the same work, we observed a very fast decay (~ 110 fs) of the Chl *a* Q_y peak. Since Chl *a* Q_y is the lowest energy bright state, we speculated about the presence of a dark state interacting with the Chl *a* Q_y state. Some part of the excitation could be transferred to this dark state from Chl *a* Q_y, thereby inducing the decay observed in the spectra. Surprisingly, we did not see such a decay component in the two-color 2D spectra reported here. However, evidences of this process would overlap with energy transfer from the Fx S_2 state. The mentioned dark state should be either a charge transfer (CT) state between Fx and Chl *a*, or a CT state between different Chl *a* molecules, or a Fx S_1/ICT state. In the latter case, it should likely involve Fx$_{blue}$, rather than Fx$_{red}$, because of the lower overall transfer efficiency.

Energy transfer schemes of the FCP, obtained from pump–probe studies [11,15,13,16], are in general consistent with the scheme proposed here, apart from a few details. The ratio of Fx S_2 to S_1/ICT and Chl *a* transfer was suggested to be 60:40% [11]. Our ratio of ~ 80 : 20 % is much closer to 74:26%, recently obtained for FCP from brown algae [16]. In the same work, the transfer from Fx S_1/ICT to Chl *a* was estimated to occur with a timescale of ≈ 2 ps, while our data shows it to be somewhat faster. These studies, however, did not emphasize the differences in the dynamics associated with Fx$_{blue}$ and Fx$_{red}$ excitation. This was performed in another pump–probe study [15], reporting timescales comparable to ours (differences could arise due to limitations of the pump–probe technique and different type of analysis), however, the absence of the relative amplitudes of the processes prevents a detailed comparison between the two schemes.

6. Conclusions

To summarize, the two color 2D spectra of fucoxanthin–chlorophyll protein revealed the existence of two spectroscopically and thus functionally different species of fucoxanthin in FCP. Performing analysis in terms of modified decay associated spectra, we found timescales and amplitudes of the relevant dynamic processes in the FCP and constructed the full scheme of energy transfer cascades. It shows that energy transfer from the "red" fucoxanthin is faster and more efficient. Nonetheless, it is striking, how the protein organization is able to bind fucoxanthins and chlorophylls, maintaining dramatically different absorption properties, in such a way, that the spectral range for photon absorption by the whole complex is significantly enhanced and, at the same time, ultrafast and efficient excitation energy cascade from all these molecules is ensured. These properties made FCP a very efficient machine to harvest blue–green photons in aquatic environments, where the light regimes are different from those encountered by terrestrial phototrophs. It is thus not surprising that diatoms which contain many carbonyl-containing carotenoid molecules, such as peridinin or fucoxanthin, in their light-harvesting antennae are the major players in modulating the O_2 and CO_2 sinks on our planet.

Acknowledgements

The research was partially funded by the European Social Fund under the Global Grant measure (grant number VP1-3.1-ŠMM-07-K-01-007). Authors acknowledge support by the LASERLAB-EUROPE

project (grant agreement no 228334, EC's Seventh Framework Programme). Work in Lund was also supported by the Swedish Research Council and Knut and Alice Wallenberg Foundation. C. B. acknowledges funding by the Deutsche Forschungsgemeinschaft (Bu 812/4-1, 5-1). C. B., A. Gall and B. R. acknowledge funding from the EU (HARVEST Marie Curie Research Training Network (PITN-GA-2009-238017)). B. R. acknowledges support from the European Research Council (ERC) through Advanced Grant, ERC-2010-AdG PHOTPROT.

References

[1] T. Brixner, J. Stenger, H.M. Vaswani, M. Cho, R.E. Blankenship, G.R. Fleming, Two-dimensional spectroscopy of electronic couplings in photosynthesis, Nature 434 (2005) 625–628.
[2] D. Zigmantas, E.L. Read, T. Mančal, T. Brixner, A.T. Gardiner, R.J. Cogdell, G.R. Fleming, Two-dimensional electronic spectroscopy of the B800–B820 light-harvesting complex, Proc. Natl. Acad. Sci. U. S. A. 103 (2006) 12672–12677.
[3] J. Dostál, F. Vacha, J. Psencik, D. Zigmantas, 2D electronic spectroscopy reveals excitonic structure in the baseplate of a chlorosome, J. Phys. Chem. Lett. 5 (2014) 1743–1747.
[4] G.S. Schlau-Cohen, T.R. Calhoun, N.S. Ginsberg, E.L. Read, M. Ballottari, R. Bassi, R. van Grondelle, G.R. Fleming, Pathways of energy flow in LHCII from two-dimensional electronic spectroscopy, J. Phys. Chem. B 113 (2009) 15352–15363.
[5] J.A. Myers, K.L.M. Lewis, F.D. Fuller, P.F. Tekavec, C.F. Yocum, J.P. Ogilvie, Two-dimensional electronic spectroscopy of the D1–D2–cyt b559 photosystem II reaction center complex, J. Phys. Chem. Lett. 1 (2010) 2774–2780.
[6] P.G. Falkowski, R.T. Barber, V. Smetacek, Biogeochemical controls and feedbacks on ocean primary production, Science 281 (1998) 200–206.
[7] C.B. Field, M.J. Behrenfeld, J.T. Randerson, P. Falkowski, Primary production of the biosphere: integrating terrestrial and oceanic components, Science 281 (1998) 237–240.
[8] D.G. Mann, The species concept in diatoms, Phycologia 38 (1999) 437–495.
[9] D. Kosumi, T. Kusumoto, R. Fujii, M. Sugisaki, Y. Iinuma, N. Oka, Y. Takaesu, T. Taira, M. Iha, H.A. Frank, H. Hashimoto, Ultrafast excited state dynamics of fucoxanthin: excitation energy dependent intramolecular charge transfer dynamics, Phys. Chem. Chem. Phys. 13 (2011) 10762–10770.
[10] M. Eppard, E. Rhiel, The genes encoding light-harvesting subunits of *Cyclotella cryptica* (*Bacillariophyceae*) constitute a complex and heterogeneous family, Mol. Gen. Genet. 260 (1998) 335–345.
[11] E. Papagiannakis, I.H.M. van Stokkum, H. Fey, C. Büchel, R. van Grondelle, Spectroscopic characterization of the excitation energy transfer in the fucoxanthin–chlorophyll protein of diatoms, Photosynth. Res. 86 (2005) 241–250.
[12] L. Premvardhan, B. Robert, A. Beer, C. Büchel, Pigment organization in fucoxanthin chlorophyll a/c2 proteins (FCP) based on resonance Raman spectroscopy and sequence analysis, Biochim. Biophys. Acta 1797 (9) (2010) 1647–1656.
[13] N. Gildenhoff, J. Herz, K. Gundermann, C. Büchel, J. Wachtveitl, The excitation energy transfer in the trimeric fucoxanthin-chlorophyll protein from *Cyclotella meneghiniana* analyzed by polarized transient absorption spectroscopy, Chem. Phys. 373 (2010) 104–109.
[14] L. Premvardhan, L. Bordes, A. Beer, C. Büchel, B. Robert, Carotenoid structures and environments in trimeric and oligomeric fucoxanthin chlorophyll a/c2 proteins from resonance Raman spectroscopy, J. Phys. Chem. B 113 (2009) 12565–12574.
[15] N. Gildenhoff, S. Amarie, K. Gundermann, A. Beer, C. Büchel, J. Wachtveitl, Oligomerization and pigmentation dependent excitation energy transfer in fucoxanthin–chlorophyll proteins, Biochim. Biophys. Acta 1797 (2010) 543–549.
[16] D. Kosumi, M. Kita, R. Fujii, M. Sugisaki, N. Oka, Y. Takaesu, T. Taira, M. Iha, H. Hashimoto, Excitation energy-transfer dynamics of brown algal photosynthetic antennas, J. Phys. Chem. Lett. 3 (2012) 2659–2664.
[17] J. Dostál, T. Mančal, R. Augulis, F. Vácha, J. Pšenčik, D. Zigmantas, Two-dimensional electronic spectroscopy reveals ultrafast energy diffusion in chlorosomes, J. Am. Chem. Soc. 134 (2012) 11611–11617.
[18] O. Bixner, V. Lukeš, T. Mančal, J. Hauer, F. Milota, M. Fischer, I. Pugliesi, M. Bradler, W. Schmid, E. Riedle, Ultrafast photo-induced charge transfer unveiled by two-dimensional electronic spectroscopy, J. Chem. Phys. 136 (2012) 204503.
[19] S. Westenhoff, D. Paleček, P. Edlund, P. Smith, D. Zigmantas, Coherent picosecond exciton dynamics in a photosynthetic reaction center, J. Am. Chem. Soc. 134 (2012) 16484–16487.
[20] A. Gelzinis, L. Valkunas, F.D. Fuller, J.P. Ogilvie, S. Mukamel, D. Abramavicius, Tight-binding model of the photosystem II reaction center: application to two-dimensional electronic spectroscopy, New J. Phys. 15 (2013) 075013.
[21] F.D. Fuller, J. Pan, A. Gelzinis, V. Butkus, S.S. Senlik, D.E. Wilcox, C.F. Yocum, L. Valkunas, D. Abramavicius, J.P. Ogilvie, Vibronic coherence in oxygenic photosynthesis, Nat. Chem. 6 (2014) 706–711.
[22] E. Romero, R. Augulis, V.I. Novoderezhkin, M. Ferretti, J. Thieme, D. Zigmantas, R.V. Grondelle, Quantum coherence in photosynthesis for efficient solar-energy conversion, Nat. Phys. 10 (2014) 676–682.
[23] D.M. Jonas, Two-dimensional femtosecond spectroscopy, Annu. Rev. Phys. Chem. 54 (2003) 425–463.
[24] J.A. Myers, K.L. Lewis, P.F. Tekavec, J.P. Ogilvie, Two-color two-dimensional Fourier transform electronic spectroscopy with a pulse-shaper, Opt. Express 16 (2008) 17420–17428.
[25] D. Abramavicius, V. Butkus, J. Bujokas, L. Valkunas, Manipulation of two-dimensional spectra of excitonically coupled molecules by narrow-bandwidth laser pulses, Chem. Phys. 372 (2010) 22–32.
[26] M. Kullmann, S. Ruetzel, J. Buback, P. Nuernberger, T. Brixner, Reaction dynamics of a molecular switch unveiled by coherent two-dimensional electronic spectroscopy, J. Am. Chem. Soc. 133 (2011) 13074–13080.
[27] N. Krebs, I. Pugliesi, J. Hauer, E. Riedle, Two-dimensional Fourier transform spectroscopy in the ultraviolet with sub-20 fs pump pulses and 250-720Â nm supercontinuum probe, New J. Phys. 15 (2013) 085016.
[28] F.D. Fuller, J.P. Ogilvie, Continuum probe two-dimensional electronic spectroscopy of the photosystem II reaction center, EPJ Web Conf. 41 (2013) 08018.
[29] T.A.A. Oliver, N.H.C. Lewis, G.R. Fleming, Correlating the motion of electrons and nuclei with two-dimensional electronic-vibrational spectroscopy, Proc. Natl. Acad. Sci. U. S. A. 111 (2014) 10061–10066.
[30] C. Büchel, Fucoxanthin–chlorophyll proteins in diatoms: 18 and 19 kDa subunits assemble into different oligomeric states, Biochemistry 42 (2003) 13027–13034.
[31] T. Brixner, I.V. Stiopkin, G.R. Fleming, Tunable two-dimensional femtosecond spectroscopy, Opt. Lett. 29 (2004) 884–886.
[32] R. Augulis, D. Zigmantas, Two-dimensional electronic spectroscopy with double modulation lock-in detection: enhancement of sensitivity and noise resistance, Opt. Express 19 (2011) 13126–13133.
[33] R. Augulis, D. Zigmantas, Detector and dispersive delay calibration issues in broadband 2D electronic spectroscopy, J. Opt. Soc. Am. B 30 (2013) 1770–1774.
[34] L. Valkunas, D. Abramavicius, T. Mančal, Molecular Excitation Dynamics and Relaxation, Wiley-VCH, Berlin, 2013.
[35] S. Mukamel, Principles of Nonlinear Optical Spectroscopy, Oxford University Press, New York, 1995.
[36] E.E. Ostroumov, R.M. Mulvaney, J.M. Anna, R.J. Cogdell, G.D. Scholes, Energy transfer pathways in light-harvesting complexes of purple bacteria as revealed by global kinetic analysis of two-dimensional transient spectra, J. Phys. Chem. B 117 (2013) 11349–11362.
[37] F. Milota, V.I. Prokhorenko, T. Mančal, H. von Berlepsch, O. Bixner, H.F. Kauffmann, J. Hauer, Vibronic and vibrational coherences in two-dimensional electronic spectra of supramolecular j-aggregates, J. Phys. Chem. A 117 (2013) 6007–6014.
[38] J. Alster, H. Lokstein, J. Dostál, A. Uchida, D. Zigmantas, 2D spectroscopy study of water-soluble chlorophyll-binding protein from *Lepidium virginicum*, J. Phys. Chem. B 118 (2014) 3524–3531.
[39] I.H. van Stokkum, D.S. Larsen, R. van Grondelle, Global and target analysis of time-resolved spectra, Biochim. Biophys. Acta 1657 (2004) 82–104.
[40] R. Byrd, P. Lu, J. Nocedal, C. Zhu, A limited memory algorithm for bound constrained optimization, SIAM J. Sci. Comput. 16 (1995) 1190–1208.
[41] R Development Core Team, R: A Language and Environment for Statistical Computing, R Foundation for Statistical Computing, Vienna, Austria, 2012.
[42] V. Balevičius Jr., A. Gelzinis, D. Abramavicius, T. Mančal, L. Valkunas, Excitation dynamics and relaxation in a molecular heterodimer, Chem. Phys. 404 (2012) 94–102.
[43] V. Balevičius Jr., A. Gelzinis, D. Abramavicius, L. Valkunas, Excitation energy transfer and quenching in a heterodimer: applications to the carotenoid–phthalocyanine dyads, J. Phys. Chem. B 117 (2013) 11031–11041.
[44] R. Croce, H. van Amerongen, Natural strategies for photosynthetic light harvesting, Nat. Chem. Biol. 10 (2014) 492–501.
[45] H. van Amerongen, R. van Grondelle, Understanding the energy transfer function of LHCII, the major light-harvesting complex of green plants, J. Phys. Chem. B 105 (2001) 604–617.
[46] N.E. Holt, J. Kennis, L. Dall'Osto, R. Bassi, G.R. Fleming, Carotenoid to chlorophyll energy transfer in light harvesting complex II from *Arabidopsis thaliana* probed by femtosecond fluorescence upconversion, Chem. Phys. Lett. 379 (2003) 305–313.
[47] V. Chukhutsina, C. Büchel, H. van Amerongen, Variations in the first steps of photosynthesis for the diatom *Cyclotella meneghiniana* grown under different light conditions, Biochim. Biophys. Acta 1827 (2013) 10–18.
[48] V.U. Chukhutsina, C. Büchel, H. van Amerongen, Disentangling two non-photochemical quenching processes in *Cyclotella meneghiniana* by spectrally-resolved picosecond fluorescence at 77 K, Biochim. Biophys. Acta 1837 (2014) 899–907.
[49] E. Songaila, R. Augulis, A. Gelzinis, V. Butkus, A. Gall, C. Büchel, B. Robert, D. Zigmantas, D. Abramavicius, L. Valkunas, Ultrafast energy transfer from chlorophyll c2 to chlorophyll a in fucoxanthin-chlorophyll protein complex, J. Phys. Chem. Lett. 4 (2013) 3590–3595.